Interlayer exchange coupling of Fe/Cr/Fe thin films on rippled substrates

M. Körner,* K. Lenz, M. O. Liedke, T. Strache, A. Mücklich, A. Keller, S. Facsko, and J. Fassbender
Institute of Ion Beam Physics and Materials Research, Forschungszentrum Dresden–Rossendorf, P.O. Box 51 01 19, 01314 Dresden, Germany

(Received 11 June 2009; revised manuscript received 22 September 2009; published 1 December 2009)

The influence of a nanoscale surface modulation periodicity of ion beam eroded substrates (ripples) on the interlayer exchange coupling in polycrystalline Fe/Cr/Fe thin films is investigated. Using 22 nm rippled substrates, we find a pronounced Néel coupling superimposed on the interlayer exchange coupling in Fe/Cr/Fe trilayers associated with a strong uniaxial anisotropy induced by the substrate topography. For longer periods the Néel contribution and uniaxial anisotropy become weaker and finally vanish in the case of a flat substrate and film. These results are obtained by applying a Stoner-Wohlfarth model on magnetic reversal loops measured by longitudinal magneto-optical Kerr effect magnetometry.

DOI: 10.1103/PhysRevB.80.214401 PACS number(s): 68.35.Ct, 68.37.−d, 75.30.Et, 75.50.Bb

I. INTRODUCTION

With the discovery of antiferromagnetic interlayer exchange coupling (IEC) in Fe/Cr/Fe trilayers by Grünberg *et al.*[1] a broad interest in magnetically coupled structures developed, which led to further discoveries such as long and short range oscillations of the interlayer exchange coupling strength with respect to the spacer thickness.[2,3] A major influence on the coupling strength, consisting of a bilinear and a biquadratic part, could be attributed to the interface roughness.[4–10] On one hand, an increasing interfacial roughness leads to a decrease in the bilinear antiferromagnetic coupling strength.[11] On the other hand, dipolar interactions are introduced to the system[12] as well as spatial fluctuations[13] both leading to an increase in the biquadratic coupling strength. Using recent ion irradiation techniques to modify the interfaces after deposition the IEC can be tuned as well.[14,15] The first calculations concerning magnetostatic coupling arising from dipolar interactions were done by Néel in 1962.[16] This so-called Néel coupling deals with two separated semi-infinite ferromagnetic layers with in-plane magnetization and sinusoidally modulated surfaces and aligns both magnetizations parallel to each other, in case of conformal interface modulation at all interfaces of the trilayer stack. Usually this is the case for stacked layer systems and has been observed in the past in several experiments on rough[11,14] as well as patterned surfaces with a step-like modulation.[14,17,18] However, only micrometer-sized surface modulations could be achieved and were investigated. The preparation of well-defined surface/interface modulations remained challenging. With the arrival of improved ion beam erosion techniques an effective tool for surface patterning on the nanometer scale became available, which allows the preparation of sinusoidally modulated surfaces (ripples).[19] As the kinetic energy of the ions is directly correlated with the ripple wavelength[14] this gives the unique possibility to selectively choose the period of the surface modulation from as low as 20 nm or as large like a few 100 nm. Furthermore, patterned magnetic layers offer a chance to study the surface contribution to the development of magnetic anisotropy on the surface topography.[20–24] The conventional IEC in Fe/Cr/Fe trilayers and multilayers has already been studied for a while,[25–27] however open questions on the interfacial influence and properties still remain.

Here, we present a quantitative analysis of the influence of sinusoidally modulated surfaces on the topographic and magnetic properties of interlayer exchange coupled Fe layers. After introducing the sample structure and experimental details in Sec. II the results are presented and discussed in Sec. III. Section IV summarizes our findings.

II. EXPERIMENTAL DETAILS

In order to investigate the influence of sinusoidally modulated (rippled) surfaces, two types of substrates were used. (i) Flat Si(100) for reference purposes and (ii) rippled substrates with ripple wavelengths of 22 and 37 nm, respectively. The latter were produced by ion beam erosion of Si(111) surfaces with a reproducibility of ± 1 nm in the wavelength. Details of the sputtering process are reported elsewhere.[28] As the substrates were transferred under atmospheric conditions from the erosion chamber to the deposition vacuum chamber, they are covered by natural oxide layers (SiO_2) of approximately 1.5–2.0 nm thickness.

Initial investigations of the surface topography were performed by atomic force microscopy (AFM) before the templates were inserted into a molecular beam epitaxy system with a base pressure of less than 10^{-10} mbar. Prior to film deposition the samples were annealed to 200 °C in order to clean the surface. Subsequently the whole stack of Cr(4 nm)/Fe(4 nm)/Cr(d_{Cr})/Fe(4 nm)/Cr(2 nm) was deposited at room temperature using an e-beam evaporator. The Cr spacer layer was prepared as a wedge with thickness, d_{Cr}, ranging from 0 to 5 nm, using a movable shutter placed between evaporator and sample. Depending on d_{Cr} the Fe layers are ferromagnetically (FM) or antiferromagnetically (AF) coupled.[3] After deposition the surface topography was imaged by *ex situ* AFM. The image processing was performed using WSXM[29] and GWYDDION[30] software. Cross-sectional transmission electron microscopy (TEM) was used to investigate the lateral layer structure. Finally, the magnetic properties were determined by means of longitudinal magneto-optical Kerr effect magnetometry (MOKE), using *s*-polarized light.

III. RESULTS AND DISCUSSION

Figure 1 shows AFM micrographs of the substrate types used. These micrographs were subsequently fast Fourier

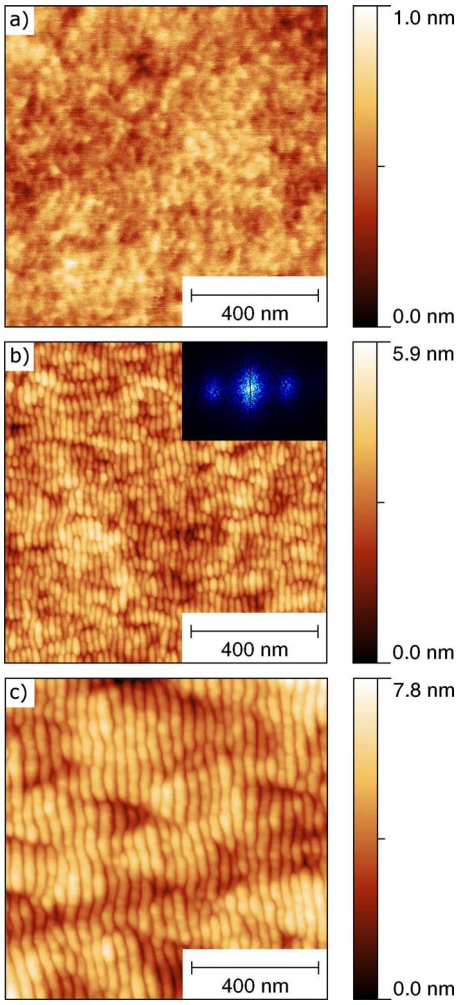

FIG. 1. (Color online) AFM micrographs of the different substrate types. (a) Si(100) covered by natural SiO_2 with $\omega=0.1$ nm, (b) rippled Si(111)/SiO_2 with a ripple wavelength of $\lambda=22$ nm and $\omega=0.7$ nm, and (c) rippled Si(111)/SiO_2 with $\lambda=37$ nm and $\omega=1$ nm. The inset of (b) shows a FFT of the surface.

transformed (FFT), which provides information about the roughness distribution. As an example the inset of Fig. 1(b) shows the FFT of the 22 nm rippled substrate. Visible are a center peak and two satellite peaks, arising from the periodically modulated, strongly anisotropic ripple surface. By measuring the distance between these peaks the ripple wavelength, λ, can be calculated. In the case of flat Si [Fig. 1(a)] only the center peak would be visible (FFT not shown) due to isotropic roughness. When comparing flat and rippled substrates an increase of the root mean square (RMS) roughness ω was observed starting from $\omega=0.1$ nm for flat Si to finally $\omega=1,0$ nm in the case of the rippled Si substrate with a wavelength of $\lambda=37$ nm. Contrary to ripples with a wavelength of $\lambda=22$ nm [see Fig. 1(b)] a periodicity of $\lambda=37$ nm as shown in Fig. 1(c) offers a much better quality with respect to the surface modulation due to fewer interrupted wave fronts. After deposition of the Fe/Cr/Fe stack the RMS roughness value, ω, slightly increases, as the values in Table I indicate, whereas the wavelength is not affected.

A better understanding of the lateral structure of the stack is provided by cross-sectional TEM measurements shown in Fig. 2. The principal structure of all samples is similar. Shown at the bottom of each image is the Si substrate, which contains the Si lattice capped by an amorphous SiO_2 layer of

TABLE I. Influence of ripple wavelength λ and film deposition on RMS roughness ω.

	Before deposition		After deposition $d_{Cr}=1.1$ nm	
Substrate	λ (nm)	ω (nm)	λ (nm)	ω (nm)
Si/SiO_2		0.1		0.6
Ripple	22	0.7	22	0.9
	37	1.0	37	1.1

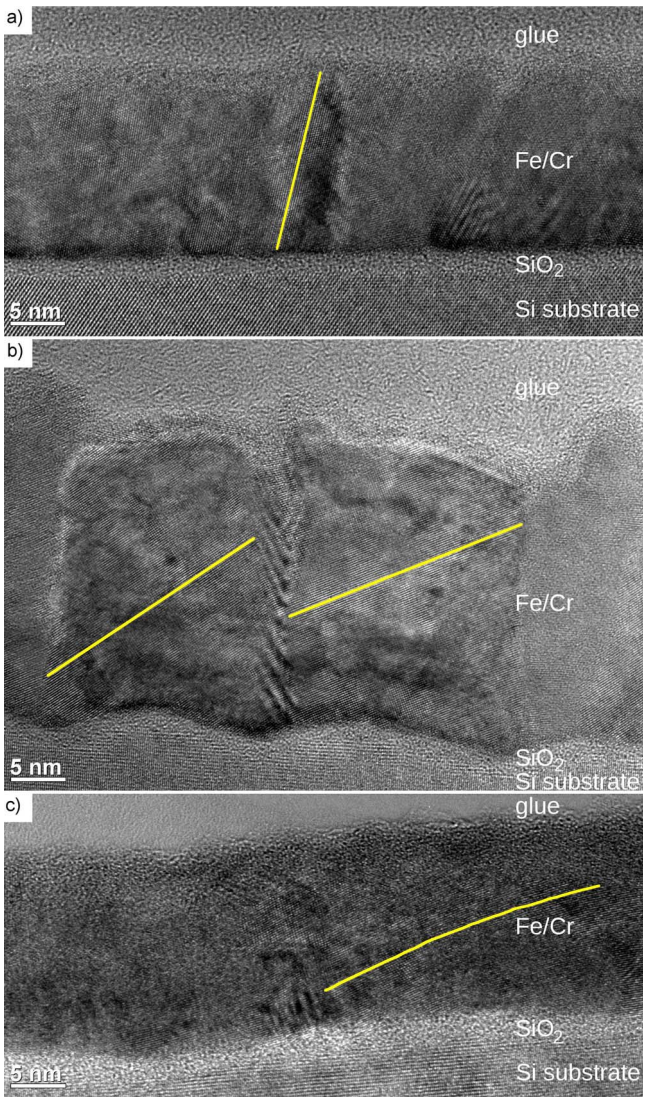

FIG. 2. (Color online) TEM cross sections of Cr(4 nm)/Fe(4 nm)/Cr(d_{Cr})/Fe(4 nm)/Cr(2 nm) on (a) flat Si/SiO_2 substrate with $d_{Cr}=1.1$ nm, (b) $\lambda=22$ nm ripples with amplitude $h=2$ nm and $d_{Cr}=10$ nm, and (c) on $\lambda=37$ nm ripples with $h=1.8$ nm and $d_{Cr}=1.1$ nm. The solid yellow lines indicate the lattice planes inside the polycrystalline stack.

about 1.6 nm. It results from natural oxidation and gives an amorphous basis for the following layers. The Fe/Cr/Fe stack, sandwiched between Cr layers follows. The bottom Cr buffer layer is needed to transform the amorphous into polycrystalline growth whereas the Cr capping layer protects the top Fe layer against oxidation. Independent of the substrate topography used, the differentiation between Fe and Cr layers in the TEM pictures is impossible, because of vanishing contrast due their similar cross sections. Moreover, the polycrystalline lattice structure, predefined by the Cr buffer, passes through the whole Fe/Cr/Fe stack without visible defects at the Fe/Cr interfaces. The fine epitaxial growth of Fe on Cr and vice versa is due to the small lattice mismatch between Fe and Cr of about 0.6% having both grown with bcc structure. The glue layer visible on top of the Cr cap layer is necessary for the TEM preparation.

By varying the substrate topography structural changes of the lattice system are induced. Crystals with various in-plane diameters in case of Si/SiO_2 substrate [see Fig. 2(a), $d_{Cr}=1.1$ nm, layer stack thickness $d=15.1$ nm] are replaced by crystals with lateral sizes comparable to the ripple wavelength of $\lambda=22$ nm [see Fig. 2(b), $d_{Cr}=10$ nm]. The relatively large spacer thickness of $d_{Cr}=10$ nm was chosen in order to validate the topographic reproducibility of the system in the limit of thick spacer layers. Increasing λ further to $\lambda=37$ nm [see Fig. 2(c), $d_{Cr}=1.1$ nm] causes a reorientation of the lattice with respect to the surface corrugation and simultaneous annihilation of the ripple-grain-size correlation. This structural change is indicated in Fig. 2 by solid yellow lines highlighting an example of one lattice plane. In both rippled samples the deposited layer stack shows the same surface modulation with respect to periodicity and amplitude of the rippled substrate.

The magnetic characterization of the samples was done by MOKE measurements. Depositing the layer system on Si/SiO_2 using a wedged Cr spacer layer, results in a variation of the saturation field H_S, shown in Fig. 3(c) in black. Only the first large peak of the oscillation of H_S is detectable. This peak extends from 0.6 nm up to 2 nm of the spacer thickness with a peak value of $H_S=3.1$ kOe at $d_{Cr}=1.1$ nm. In addition to H_S the negative sum of bilinear and biquadratic coupling strength $-(J_1+J_2)$ for the AF coupled state is shown as red circles in Fig. 3(c). The latter was achieved by applying a Stoner-Wohlfarth model to the measured hysteresis loops. Therefore the energy density

$$F(\varphi_1,\varphi_2) = -J_1\cos(\varphi_1-\varphi_2) - J_2\cos^2(\varphi_1-\varphi_2) - \mu_o H[d_1M_1\cos(\varphi_1) + d_2M_2\cos(\varphi_2)], \quad (1)$$

was minimized with respect to the angles φ_i between the corresponding magnetizations M_i of the two Fe layers ($i=1,2$) and the applied external field H. As an assumption the Fe layers were treated as uniformly magnetized. Equation (1) consists of the coupling energy density with the bilinear (biquadratic) coupling constant J_1 (J_2) and the Zeeman term, respectively. The latter covers the interaction of the magnetic layer i of thickness d_i with the external field H. Usually within the IEC model (constants J_1 and J_2) Cr is treated as non magnetic spacer layer. In our case this model provides the best agreement with the theory. Contrary to that Slonczewski's proximity model treats Cr as magnetic layer taking the antiferromagnetic behavior into account.[13] This leads to additional two monolayer period oscillations of the coupling strength and an asymptotic saturation of the magnetization in an external field. However, by using a polycrystalline structure the proximity magnetism of Cr is suppressed. Moreover, the two monolayer oscillations are damped due to rough interfaces.[31] Fig. 3(a) shows such an AF coupled loop around the maximum of the AF coupling strength ($J_1=-0.68$ mJ/m^2, $J_2=-0.09$ mJ/m^2) for $d_{Cr}\approx 1.1$ nm. The asymptotic saturation behavior expected from the proximity model is only very weakly distinct. Figure 3(b) shows the corresponding FM coupled case with a regular hysteresis loop for $d_{Cr}=2$ nm.

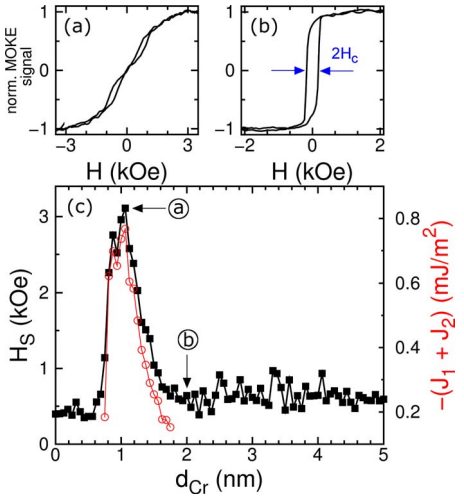

FIG. 3. (Color online) Magnetization reversal loops for (a) AF coupling at 1.1 nm and (b) FM coupling at 2 nm Cr spacer thickness. (c) Saturation field H_S and AF coupling strength $-(J_1+J_2)$ of Fe/Cr/Fe as a function of Cr spacer layer thickness, deposited on amorphous Si/SiO_2.

To investigate the angular dependence of the magnetic anisotropy, MOKE measurements were performed and the sample was rotated while keeping the direction of the applied external magnetic field as well as the direction of the incident laser beam constant. The results for trilayers on flat Si/SiO_2 substrate are shown in Fig. 4(a). In the case of AF coupling ($d_{Cr}=1.1$ nm) the total AF coupling strength $-(J_1+J_2)$ is displayed whereas for FM coupling ($d_{Cr}=2$ nm) the magnetic anisotropy energy (MAE) is shown, because the FM coupling strength cannot be resolved from MOKE measurements. The MAE is derived from the area of the hysteresis loop assuming the bulk iron saturation magnetization of 1710 kA/m. Both data sets, FM and AF coupled, indicate an isotropic behavior of the magnetic properties, which matches the isotropic roughness distribution seen using AFM.

The magnetic behavior changes markedly if the Fe/Cr stack is deposited on rippled substrates. Using $\lambda=22$ nm rippled substrate MOKE angle-dependent measurements were performed on the deposited stack. These are presented in Figs. 4(b) and 4(c). Both coupling states, AF in Fig. 4(b) and FM in Fig. 4(c), are strongly anisotropic as the plots of the coercivity and the MAE show. To explain the measure-

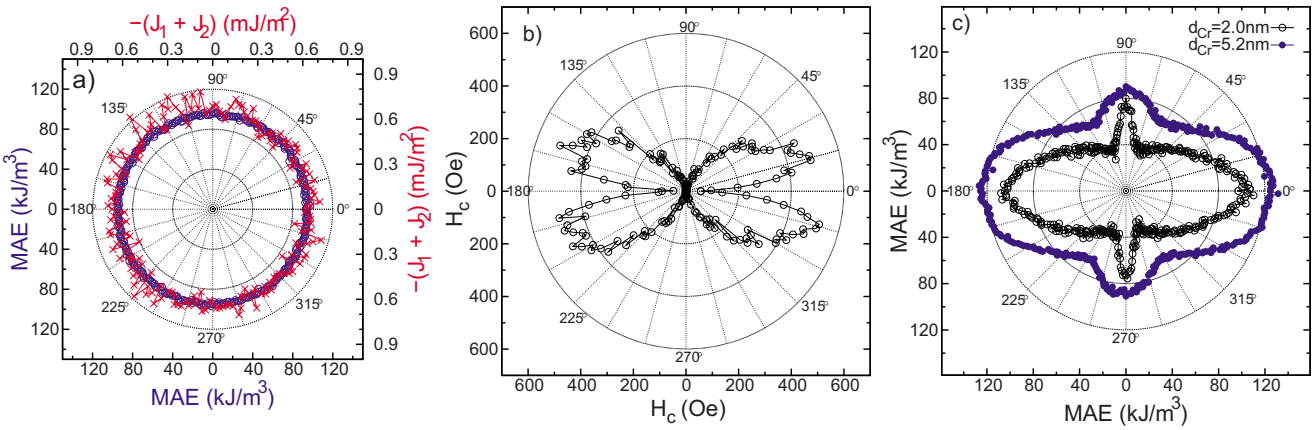

FIG. 4. (Color online) Angular dependence of (a) the MAE for the trilayers on flat Si/SiO_2 in the FM coupled state (d_{Cr}=2 nm, blue circles) and calculated coupling strength $-(J_1+J_2)$ for AF coupling (d_{Cr}=1.1 nm, red crosses). Angular dependence of (b) H_C for AF coupled (d_{Cr}=1.1 nm) and (c) of the MAE for FM coupled trilayers (black open circles: d_{Cr}=2 nm, blue full circles: d_{Cr}=5.2 nm), all on λ =22 nm rippled substrates.

ment we applied a Stoner-Wohlfarth model on the AF coupled state.

The surface modulation of the rippled substrates shown in Figs. 1(b) and 1(c) suggest the occurrence of Néel coupling. Néel proposed a model that describes the coupling of two semi-infinite layers with a pinned layer (M_1) and a free-layer (M_2), separated by a nonmagnetic spacer layer of thickness d_{Cr}.[16] In this model, the magnetization of the pinned layer is not able to follow the surface modulation, which results in creation of magnetic dipoles at the outer surfaces of the magnetic layers and thus to a magnetic stray field, which in turn aligns the free layer with the pinned one. The alignment strongly depends on the correlation of the interfaces between the two ferromagnetic layers.[32] A ferromagnetic alignment is achieved for an in phase roughness modulation of the interfaces, sketched in Fig. 5. The original Néel model was extended by Zhang and White[32] with respect to finite thicknesses (d_1 and d_2) of the FM layers and results in a contribution to the bilinear coupling strength analytically given by Kools *et al.*:[33]

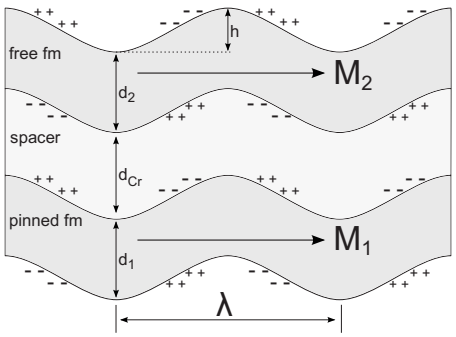

FIG. 5. Sketch of the extended Néel model for rough interfaces with wavelength λ and in-phase correlation (Ref. 32). The pinned FM layer with magnetization M_1 induces magnetic dipoles (indicated by +/−), which align the magnetization M_2 collinearly (FM coupling).

$$J_{1,\text{theor.}}^{\text{Néel}} = \frac{\mu_0 \pi^2}{\sqrt{2}} \frac{h^2}{\lambda} M_1 M_2 \exp\left(-2\pi\sqrt{2}\frac{d_{\text{Cr}}}{\lambda}\right) \times \left[1 - \exp\left(-2\pi\sqrt{2}\frac{d_1}{\lambda}\right)\right] \times \left[1 - \exp\left(-2\pi\sqrt{2}\frac{d_2}{\lambda}\right)\right], \quad (2)$$

where h is the amplitude and λ the wavelength of the ripples. The first term is the original Néel term whereas the other terms cover the finite thicknesses of the layers. Taking values from the experiment (M_1=M_2=1710 kA/m, h=2 nm, λ =22 nm, d_1=d_2=4 nm, and d_{Cr}=1.1 nm) the extended Néel model predicts a ferromagnetic coupling strength of $J_{1,\text{theor.}}^{\text{Néel}}$=0.14 mJ/m². Note that this prediction is only valid for trilayer systems with one fixed and one free magnetization. In the present experiment both magnetizations are free and can influence each other, which results in a self consistent problem, whose upper limit can be given by

$$J_{1,\text{theor.}}^{\text{Néel,free}} = 2J_{1,\text{theor.}}^{\text{Néel}} = 0.28 \ \frac{\text{mJ}}{\text{m}^2} \quad (3)$$

Furthermore, Eq. (2) assumes a perpendicular alignment of M_1 and M_2 with respect to the ripple wavefront. By applying an external field and due to IEC an arbitrary in-plane orientation of the magnetizations with respect to the ripple wavefront is possible. Thus, the projections of the interacting magnetizations perpendicular to the ripple wavefront have to be taken into account. Treating interlayer exchange and Néel coupling as two superimposing effects the total bilinear coupling strength can be written as

$$J_1 = J_1^0 + J_{1,\text{exp}}^{\text{Néel}}[|\sin(\varphi_1 - \Phi)\sin(\varphi_2 - \Phi)|]. \quad (4)$$

Φ represents the angle between the externally applied field H and a preferential sample direction, namely, a vector parallel to the ripple wavefront. J_1^0 is the bilinear coupling strength occurring on flat substrates without Néel coupling and $J_{1,\text{exp.}}^{\text{Néel}}$

is the corresponding Néel coupling strength on rippled surfaces.

In addition to Néel coupling, the uniaxial anisotropy as described by the free-energy density

$$F_{\mathrm{ani}}(\varphi_1,\varphi_2,\Phi) = K_{2\|}[d_1 \sin^2(\varphi_1-\Phi) + d_2 \sin^2(\varphi_2-\Phi)] \tag{5}$$

can be expected, where $K_{2\|}$ is the uniaxial anisotropy constant. Finally, the energy density of Fe/Cr/Fe on rippled substrates reads

$$F_{\mathrm{ripple}}(\varphi_1,\varphi_2,\Phi) = F(\varphi_1,\varphi_2) + F_{\mathrm{ani}}(\varphi_1,\varphi_2,\Phi). \tag{6}$$

In order to evaluate $F(\varphi_1,\varphi_2)$ it is necessary to use Eq. (1) where J_1 is substituted by Eq. (4). Using the above mentioned values for the parameters M_i and d_i the coupling constants J_1^0, $J_{1,\mathrm{exp}}^{\mathrm{Néel}}$, and J_2 as well as the uniaxial anisotropy constant $K_{2\|}$ can be extracted by fitting the model to the data. The fit of the four parameters to the measured curves was done alternatingly for fields parallel ($\Phi=0°$) and perpendicular ($\Phi=90°$) to the ripple wave front and results in

$$J_1^0 = -0.60(3)\ \frac{\mathrm{mJ}}{\mathrm{m}^2}, \quad J_{1,\mathrm{exp}}^{\mathrm{Néel}} = 0.17(2)\ \frac{\mathrm{mJ}}{\mathrm{m}^2},$$

$$J_2 = -0.18(2)\ \frac{\mathrm{mJ}}{\mathrm{m}^2}, \quad K_{2\|} = 70(5)\times 10^3\ \frac{\mathrm{J}}{\mathrm{m}^3}.$$

Figures 6(a) and 6(c) show the obtained results for $\Phi=0°$ and $\Phi=90°$, respectively. To check the prediction of the model a third simulation with $\Phi=44°$ was done, depicted in Fig. 6(b). In every case the simulation reproduces the measurement very well. The fact that the simulated curves do not show any hysteretic behavior arises from the chosen minimization method for the free energy density, where always the global minimum was taken. Hence, only coherent rotation processes are described by the model, neglecting any domain wall motion. This assumption fits very well in case of a hard axis loop, where the energy state of the system has only one minimum. However, the chosen method cannot reproduce any coercivity in easy axis loops. In any case these effects are also influenced by domain wall motion processes and would be overestimated by coherent rotation.

To extract the influence of the 22 nm rippled substrates on the IEC of Fe/Cr/Fe in the AF coupled state ($d_{\mathrm{Cr}}=1.1$ nm) the values from the rippled system are compared with the reference measurement on flat SiO_2 substrate (Fig. 3). First of all an increase of the biquadratic coupling strength J_2 is observed, which has—as proven by AFM measurements (Table I)—its origin in the increased roughness of the system.[12] A comparison of the bilinear coupling strength is more complicated due to the Néel coupling which arises on rippled substrates. The pure bilinear coupling J_1^0 is still comparable to the bilinear coupling J_1 for flat interfaces. Certainly, the observed Néel coupling is superimposed [Eq. (4)] onto the regular IEC, which leads to a reduction of the total bilinear coupling strength, if the external static field is applied perpendicularly to the ripple wavefront ($\Phi=90°$) and the Fe layers are AF coupled ($\varphi_1=0°$, $\varphi_1=180°$, or vice versa). Thus one obtains $J_1^{tot}=-0.43\frac{\mathrm{mJ}}{\mathrm{m}^2}$. If the AF coupled

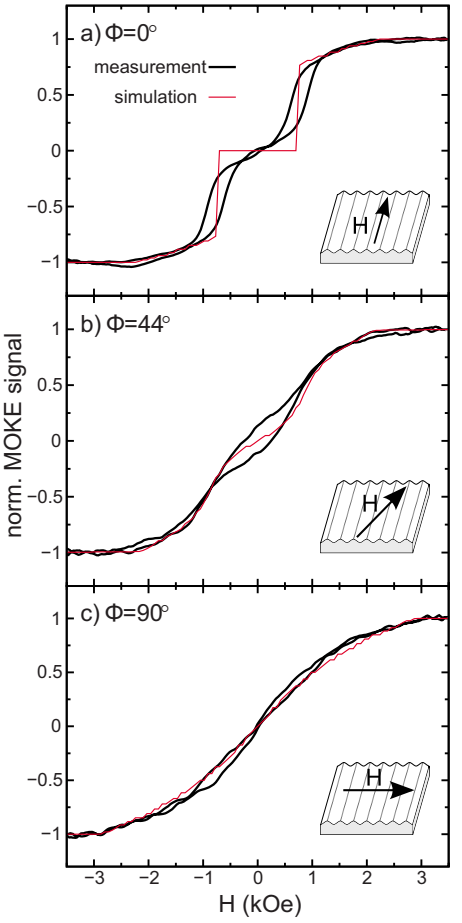

FIG. 6. (Color online) Measured (thick black) and simulated (thin red) magnetization reversal curve of Fe/Cr/Fe deposited on $\lambda=22$ nm ripples with $d_{\mathrm{Cr}}=1.1$ nm. Φ denotes the angle between H and the wavefront of the ripples.

films' magnetizations are parallel to the ripple wavefront ($\Phi=0°$), the total bilinear coupling strength is unaffected ($J_1^{tot}=J_1^0$), because none of the dipoles, necessary for Néel coupling are created.

The observed Néel coupling $J_{1,\mathrm{exp}}^{\mathrm{Néel}}$ is just half of the value predicted for an upper limit in Eq. (3). This deviation arises on the one hand from the mutual interaction of both Fe layers. On the other hand the assumption of uniformly magnetized Fe layers may break down in polycrystalline films. As a consequence the magnetization can follow the surface corrugation partially, which lowers the strength of the created dipoles and finally reduces the Néel coupling.

Applying the model introduced in this work fails in the case of FM coupling depicted in Fig. 4(c), because the magnetization reversal loop of FM coupled Fe layers does not change its shape with varying ferromagnetic coupling strength. However, the influence of Néel coupling is still visible. Assuming FM coupling ($\varphi_1=\varphi_2=\varphi$) the overall energy density of the system [Eqs. (1) and (4)–(6)] would lead to a quadratic sinusoidal angle dependence. In contrast to this Fig. 4(c) shows additionally peaks at $\varphi=90°$ and $\varphi=270°$. Such peaks are observable in some materials along a hard axis direction of the loop within a small angular range. In our case this angular range is spread up due to the inhomogeneous ripple wavefront distribution.[34,35]

By repeating the angle dependent experiments on ripples with $\lambda = 37$ nm only a very weak Néel coupling as well as magnetic anisotropy is visible, which makes an evaluation with the introduced model impossible. Using Eqs. (2) and (3) the expected Néel coupling strength of 4 nm thick Fe layers separated by 1.1 nm Cr on 37 nm ripples with $h = 1.8$ nm results in $J_{1,\mathrm{theor}}^{\mathrm{Néel,free}} = 0.1\ \mathrm{mJ/m^2}$ and, thus, is much weaker than in the case of 22 nm ripples. Furthermore, the lattice structure of the Fe/Cr/Fe stack has changed, as the TEM images have shown [Fig. 2(c)]. This has a direct impact on the magnetic anisotropy. Finally, the increased surface modulation eases an adaptation of the magnetization with respect to the surface corrugation and thus influences the magnetic anisotropy.

IV. SUMMARY

The interlayer exchange coupling in thin Fe/Cr/Fe trilayers grown on flat and rippled SiO_2 substrates has been investigated by MOKE. Néel type coupling, as well as uniaxial magnetic anisotropy, has to be added to the bilinear and biquadratic IEC contributions in order to model the hysteresis curves of trilayers grown on nanoscale rippled substrates. The bilinear coupling strength is similar for flat and rippled substrates, whereas the biquadratic contribution is a factor of two larger. The Néel coupling contribution is of the same order of magnitude as the biquadratic IEC contribution. Thus, by using rippled substrates created by ion beam erosion, it is possible to tailor the interlayer exchange coupling strength apart from adjusting the spacer thickness only. This adds another degree of freedom to optimize magnetic properties for spintronics applications.

ACKNOWLEDGMENTS

This work has been supported by the Deutsche Forschungsgemeinschaft (Grant No. FA 314/6-1).

*m.koerner@fzd.de

[1] P. Grünberg, R. Schreiber, Y. Pang, M. B. Brodsky, and H. Sowers, Phys. Rev. Lett. **57**, 2442 (1986).
[2] S. S. P. Parkin, N. More, and K. P. Roche, Phys. Rev. Lett. **64**, 2304 (1990).
[3] J. Unguris, R. J. Celotta, and D. T. Pierce, Phys. Rev. Lett. **67**, 140 (1991).
[4] E. M. Ho, A. C. Daykin, and A. K. Petford-Long, J. Appl. Phys. **79**, 6292 (1996).
[5] C.-H. Chang and T.-M. Hong, Phys. Rev. B **79**, 054415 (2009).
[6] D. T. Pierce, J. Unguris, R. J. Celotta, and M. D. Stiles, J. Magn. Magn. Mater. **200**, 290 (1999).
[7] D. T. Pierce, J. A. Stroscio, J. Unguris, and R. J. Celotta, Phys. Rev. B **49**, 14564 (1994).
[8] C. M. Schmidt, D. E. Bürgler, D. M. Schaller, F. Meisinger, and H.-J. Güntherodt, Phys. Rev. B **60**, 4158 (1999).
[9] J. C. Slonczewski, Phys. Rev. Lett. **67**, 3172 (1991).
[10] M. Rührig, R. Schäfer, A. Hubert, R. Mosler, J. A. Wolf, S. Demokritov, and P. Grünberg, Phys. Status Solidi A **125**, 635 (1991).
[11] D. Kumar and A. Gupta, Hyperfine Interact. **160**, 165 (2005).
[12] S. Demokritov, E. Tsymbal, P. Grünberg, W. Zinn, and I. K. Schuller, Phys. Rev. B **49**, 720 (1994).
[13] J. C. Slonczewski, J. Magn. Magn. Mater. **150**, 13 (1995).
[14] J. Fassbender, T. Strache, M. O. Liedke, D. Markó, S. Wintz, K. Lenz, A. Keller, S. Facsko, I. Mönch, and J. McCord, New. J. Phys. (to be published).
[15] S. Blomeier, P. Candeloro, B. Hillebrands, B. Reuscher, A. Brodyanski, and M. Kopnarski, J. Magn. Magn. Mater. **310**, 2353 (2007).
[16] L. Néel, C. R. Acad. Sci. **255**, 1545 (1962); **255**, 1676 (1962).
[17] J. Zhang and R. M. White, J. Appl. Phys. **79**, 5113 (1996).
[18] P. Fuchs, U. Ramsperger, A. Vaterlaus, and M. Landolt, Phys. Rev. B **55**, 12546 (1997).
[19] W. L. Chan and E. Chason, J. Appl. Phys. **101**, 121301 (2007).
[20] R. Moroni, D. Sekiba, F. Buatier de Mongeot, G. Gonella, C. Boragno, L. Mattera, and U. Valbusa, Phys. Rev. Lett. **91**, 167207 (2003).
[21] H. Hofsäss, F. Rotter, M. Uhrmacher, K. Zhang, C. Ronning, and J. Krauser, Surf. Coat. Technol. **201**, 8477 (2007).
[22] K. Zhang, M. Uhrmacher, H. Hofsäss, and J. Krauser, J. Appl. Phys. **103**, 083507 (2008).
[23] D. Sekiba, R. Moroni, G. Gonella, F. Buatier de Mongeot, C. Boragno, L. Mattera, and U. Valbusa, Appl. Phys. Lett. **84**, 762 (2004); F. Bisio, R. Moroni, F. Buatier de Mongeot, M. Canepa, and L. Mattera, Phys. Rev. Lett. **96**, 057204 (2006).
[24] M. O. Liedke, B. Liedke, A. Keller, B. Hillebrands, A. Mücklich, S. Facsko, and J. Fassbender, Phys. Rev. B **75**, 220407(R) (2007).
[25] J. Grabowski, M. Przybylski, M. Nyvlt, and J. Kirschner, J. Appl. Phys. **104**, 113905 (2008).
[26] A. A. Rzhevsky, B. B. Krichevtsov, D. E. Bürgler, and C. M. Schneider, Phys. Rev. B **75**, 144416 (2007).
[27] D. I. Kholin, A. B. Drovosekov, S. O. Demokritov, M. Rickart, and N. M. Kreines, Phys. Met. Metallogr. **101**, S67 (2006).
[28] A. Keller, S. Roßbach, S. Facsko, and W. Möller, Nanotechnology **19**, 135303 (2008).
[29] I. Horcas, R. Fernandez, J. M. Gomez-Rodriguez, J. Colchero, J. Gomez-Herrero, and A. M. Baro, Rev. Sci. Instrum. **78**, 013705 (2007).
[30] www.gwyddion.net.
[31] P. Bruno and C. Chappert, Phys. Rev. Lett. **67**, 1602 (1991).
[32] J. Zhang and R. M. White, IEEE Trans. Magn. **32**, 4630 (1996).
[33] J. C. S. Kools, W. Kula, D. Mauri, and Tsann Lin, J. Appl. Phys. **85**, 4466 (1999).
[34] G. A. Müller, R. Gupta, K.-P. Lieb, and P. Schaaf, Appl. Phys. Lett. **82**, 73 (2003).
[35] K. Zhang, R. Gupta, G. A. Müller, P. Schaaf, and K. P. Lieb, Appl. Phys. Lett. **84**, 3915 (2004).